Lawrence Berkeley National Laboratory
Energy Geosciences

Title
Multi-Step Crystallization of Barium Carbonate: Rapid Interconversion of Amorphous and Crystalline Precursors

Authors
Whittaker, Michael L
Smeets, Paul JM
Asayesh-Ardakani, Hasti
et al.

Multi-Step Crystallization of Barium Carbonate: Rapid Interconversion of Amorphous and Crystalline Precursors

Michael L. Whittaker, Paul J. M. Smeets, Hasti Asayesh-Ardakani, Reza Shahbazian-Yassar, and Derk Joester*

* Dr. M. L. Whittaker, Dr. P. J. M. Smeets, Prof. D. Joester -- Department of Materials Science and Engineering Northwestern University 2220 Campus Drive, Evanston, IL 60208 (USA) E-mail: d-joester@northwestern.edu

Dr. H. Asayesh-Ardakani, Prof. R. Shahbazian-Yassar Department of Mechanical and Industrial Engineering University of Illinois at Chicago 842 W. Taylor Street, Chicago, IL 60607 (USA)

Abstract

The direct observation of amorphous barium carbonate (ABC), which transforms into a previously unknown barium carbonate hydrate (herewith named gortatowskite) within a few hundred milliseconds of formation, is described. In situ X-ray scattering, cryo-, and low-dose electron microscopy were used to capture the transformation of nanoparticulate ABC into gortatowskite crystals, highly anisotropic sheets that are up to 1 μm in width, yet only about 10 nm in thickness. Recrystallization of gortatowskite to witherite starts within 30 seconds. We describe a bulk synthesis and report a first assessment of the composition, vibrational spectra, and structure of gortatowskite. Our findings indicate that transient amorphous and crystalline precursors can play a role in aqueous precipitation pathways that may often be overlooked owing to their extremely short lifetimes and small dimensions. However, such transient precursors may be integral to the formation of more stable phases.

Introduction

Barium carbonate has recently attracted attention for the complex yet controllable nano- and microstructures that can be precipitated under far-from-equilibrium conditions.[1-3] Remarkably similar to the fossilized remains of putative life forms, these materials provide evidence that a high degree of control over the crystallization process can be exerted without organic molecules.[4] Mechanisms that underlie the formation of $BaCO_3$ in these systems exhibit some similarities to pathways of $CaCO_3$ crystallization, including the formation of amorphous precursors.[5, 6] "Liquid-like" precipitates can form prior to crystallization of both $CaCO_3$ and $BaCO_3$ in confinement[7, 8] or in the presence of charged polymeric additives.[9] Solid amorphous calcium barium carbonate (ACBC) with equal parts barium and calcium have been synthesized.[10] Intracellular calcium- and barium-containing amorphous carbonate precipitates have recently been found in many species of cyanobacteria,[11] and particles of macromolecule-stabilized amorphous barium carbonate (ABC) form in media containing suspended bacteria.[12] However, there are notable differences between precipitation pathways in $CaCO_3$ and $BaCO_3$ systems.

Unlike amorphous carbonates of magnesium, calcium, manganese, iron, zinc, copper, cobalt, and radium,[13-15] ABC has not been synthesized in bulk. ACBC with barium in excess of about 55 % cation fraction crystallizes rapidly,[16] and no evidence of ABC was observed in synthetic liposomes,[17] which reduce the rate of crystallization of ACC.[18] Therefore precipitation pathways in the $BaCO_3$ system may differ from those commonly observed in the $CaCO_3$ system.

Evidence for amorphous barium carbonate (ABC) was sought using in situ synchrotron X-ray scattering. High time resolution ($\Delta t=100$ ms after 10 ms dead time) was achieved by mixing 500 µL each of aqueous solutions of $BaCl_2$ (1 M) and $NaHCO_3$ (1 M) in a stopped-flow device, and passing the solution through a thin walled quartz capillary ($d_i=0.8$ mm; $d_o=1.0$ mm) in the X-ray beam path. Wide-angle (WAXS), medium-angle (MAXS), and small-angle (SAXS) X-ray scattering patterns were simultaneously acquired on three separate detectors (Supporting Figure 1). Combined, the detectors capture scattered photons with scattering vector, q, over the range from 0.0020 to 4.50 Å^{-1}, corresponding to a real space distance d from about 0.1–300 nm. This enabled a detailed analysis of the evolution of the crystallinity and shape of precipitates at very early time points.
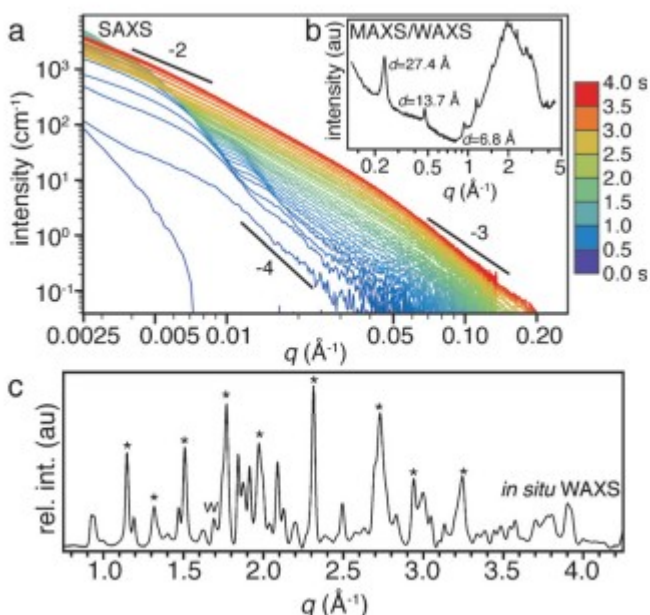

Figure 1

Simultaneously recorded, radially integrated X-ray scattering patterns of barium-carbonate rich solutions. a) SAXS patterns, acquired at 100 ms intervals. b) MAXS and WAXS patterns at 5.0 s. c) Background-corrected WAXS pattern acquired at $t=1$ min (1000 ms acquisition time). Peaks marked with an asterisk indicate those also observed in WAXS patterns recorded at high time resolution (75 ms acquisition time). A minor amount of witherite is present ("w" marks the position of the (111) peak).

While WAXS patterns showed only diffuse scattering between $q=0.8–4.5$ Å^{-1} at time points immediately following mixing ($t<1$ s, Supporting Figure 2), signal intensity in SAXS increased and displayed a characteristic oscillation (ringing) that is typical for isotropic spheres with low polydispersity (Figure 1

a).[19] This is a strong indication for the rapid formation of compact amorphous nanoparticles. Indeed, fitting of SAXS data at time points between 0.2 s and 1.0 s indicated that roughly isotropic particles grew from 40 nm to 70 nm in radius (Supporting Figure S3). At the same time, the Porod slope at $q > 0.02$ $Å^{-1}$ increased from -4.0 to -3.0, suggesting that growth of the initially compact particles resulted in a rough, surface fractal-like structure (Supporting Information, Figure S4).

Between 1.0 and 4.0 s, ringing in SAXS patterns was progressively dampened. The Porod slope approached -2 at low q and -3 at high q (Figure 1 a). This is consistent with scattering from very thin disks or sheets. Fitting of SAXS data using a two-level unified fit model[20] in the Irena software package[21] indicated that the sheets were 13.3±7.5 nm thick (Supporting Information). Over the same time, Bragg peaks emerged in WAXS patterns (Supporting Figure 2), indicating that the thin sheets were crystalline. At later times (>5 s), further strong Bragg peaks at $q = 0.48$ $Å^{-1}$ and 0.24 $Å^{-1}$ emerged in MAXS patterns, corresponding to d-spacing of 13.1 Å, and 26.2 Å (Figure 1 b).

WAXS patterns were not consistent with witherite, any known metastable $BaCO_3$ phase, or a combination thereof.[22-26] To better characterize this new phase, scattering data with higher resolution in q were acquired, using an acquisition time of 1 s at an interval of 60 s. For this purpose, 1 M aqueous $BaCl_2$ (1 mL) and 1 M aqueous $NaHCO_3$ (1 mL) were mixed ex situ, stirred gently for 30 s, and pipetted into the quartz capillary in the beam path. This procedure was necessary to avoid CO_2 bubbles that formed after about 5–10 s in the stopped-flow mixing device and displaced the solution from the beam path, terminating the experiment.

Background-corrected WAXS patterns recorded under these conditions showed a number of sharp Bragg peaks even at the earliest time point (1 min, Figure 1 c), including all peaks observed in patterns recorded with higher time resolution. A small amount of witherite was also present, and the intensity and number of peaks associated with witherite increased relative to that of the new phase over the next 24 minutes (Supporting Information, Figure S5). When the capillary was cleared with air, all diffraction peaks disappeared, indicating that the precipitation products were not tightly associated with the wall of the capillary. Taken together, the scattering data provides strong evidence that two metastable intermediates, ABC and a new crystalline phase, form prior to witherite under the conditions examined.

Owing to the short lifetime of the metastable crystalline material in solution, a bulk synthesis procedure was established. The method was similar to that described previously for the precipitation of amorphous carbonates.[27] Briefly, ice cold aqueous solutions of 1 M $BaCl_2$ and 1 M $NaHCO_3$ were rapidly mixed, filtered, washed with cold (ca. 0 °C) water, and dried under vacuum at ambient temperature. Power X-ray diffractograms (pXRD) of the resulting material were nearly indistinguishable from that obtained from in situ WAXS

(Supporting Information, Figure S6), confirming that the transient crystalline phase observed in solution was preserved upon quenching and drying.

SEM-energy dispersive spectroscopy (SEM-EDS) of bulk powders confirm that they contain carbon, oxygen, and barium, but no sodium or chlorine (Supporting Information, Figure S7). Thermogravimetric analysis (TGA) further revealed the presence of structural water (Supporting Information, Figure S8) consistent with a chemical formula of $BaCO_3 \cdot H_2O$.

The presence of structural water was confirmed using vibrational spectroscopy (Figure 2). All modes were similar to those found in calcium carbonate hydrates.[28] A broad peak at 683 cm^{-1} in IR spectra is attributed to lattice water. Another broad peak at 1653 cm^{-1} corresponds to H_2O bending modes, and at least two very broad OH stretching modes are observed, centered at approximately 3409 and 3470 cm^{-1}. Only the OH stretching mode at 3409 cm^{-1} is Raman active (Supporting Information, Figure S9). All water modes are significantly broadened, with asymmetric peaks or shoulders. This indicates that there may be several inequivalent lattice water sites and/or surface adsorbed water, and that some of these sites may be disordered.
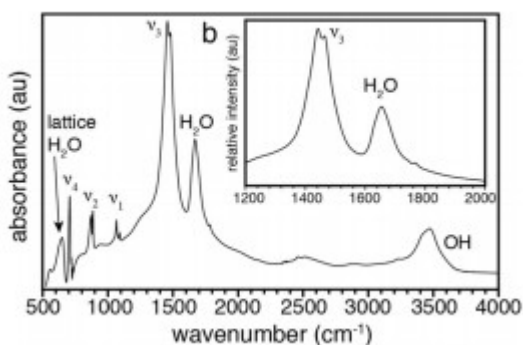

Figure 2

Vibrational spectroscopy of gortatowskite. IR spectra show the typical internal carbonate modes (ν_1–ν_4) and confirm the presence of structural water.

Internal carbonate modes, including the ν_1 (symmetric stretch), ν_2 (asymmetric bend), ν_3 (asymmetric stretch), and ν_4 (asymmetric bend) were all active in both Raman and IR (Figure 2, Supporting Information, Figure S9). All four were split, indicating that there are multiple inequivalent carbonate sites in the crystal structure. For example, the Raman ν_1 exhibited at least five distinct Gaussian contributions (Supporting Information, Figure S9).

To better understand the formation of this phase, solutions were plunge-frozen at the earliest time points accessible to us by this method (<5 s) and characterized using cryogenic scanning TEM (cryo-STEM). Images taken with high-angle annular dark-field (HAADF) contrast revealed approximately isotropic particles with dense cores and a rough surface, consistent with in situ SAXS data at 2–4 s (Figure 3 a). At later time points (5–10 s), aggregates of ribbons or thin platelets were observed (Figure 3 b). Quenching after 10 s

produced faceted sheets that extend up to 1 µm in the lateral direction (Figure 3 c). These sheets appear to align face-to-face. After approximately 30 s, acicular witherite crystallites appeared (Supporting Information, Figure S10).
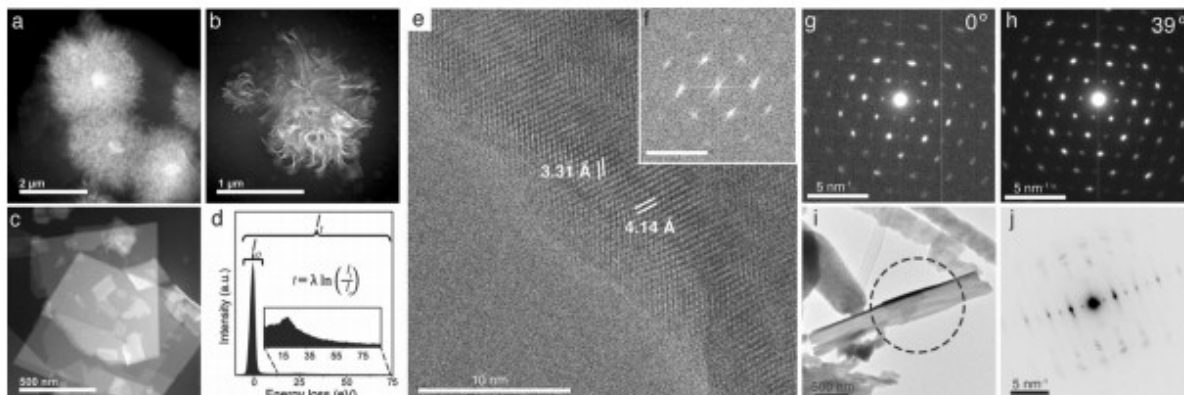

Figure 3

Formation and characterization of gortatowskite precipitates. a)–c) Cryo-STEM-HAADF image of precipitates in solutions quenched by plunge-freezing within about 10 s of inducing supersaturation. a) initial precipitates, b) platelet formation, and c) dispersion and growth. d)–j) Electron microscopy characterization of bulk precipitates. d) EELS spectrum of gortatowskite used to calculate the thickness of individual platelets. e) Aberration-corrected HR-STEM-ADF image of a platelet formed by bulk precipitation, showing lattice fringes over the entire crystallite. f) FFT of (e). g),h) SAED patterns of bulk-synthesized precipitates at 0° and 39° tilt angles, showing minimal qualitative change in the diffraction pattern. i) Bright field TEM image of of bulk-synthesized precipitate displaying the edge-on view of a precipitate stack with j) SAED taken from the area in the dashed circle.

Bulk powders imaged at ambient temperature were also composed of thin sheets (Supporting Information, Figure S6). The thickness of individual sheets was 10.5±2.5 nm (Figure 3 d), as determined using electron energy-loss spectroscopy (EELS) in ambient-temperature STEM (Supporting Information). In TEM, selected-area electron diffraction (SAED) patterns that were recorded with the sheets in a "face-on" orientation did not change significantly when the stage was tilted up to 39°. This is a hallmark of very thin crystals (Figure 3 g,h).[29] In the rare case that stacks of platelets were oriented "edge-on", strong diffraction in the "in-plane" direction is observed, while only faint and diffuse features at large reciprocal lattice vectors (small d-spacing) appeared in the stacking direction (Figure 3 i,j). Streaks perpendicular to the "in-plane" diffraction spots suggest that the d-spacing in the stacking direction is much larger than that in-plane.

Low-dose (ca. 10–20 e$^-$ [Å s]$^{-1}$), high-resolution aberration corrected STEM in annular dark field (ADF) mode with an accelerating voltage of 80 kV revealed lattice fringes that extended across the entire precipitate (Figure 3 e). Fast Fourier transform (FFT) analysis of TEM lattice fringes (Figure 3 f) confirmed that the particles were single crystals. Lattice spacing of 4.14 Å, with "AB" stacking, and 3.31 Å, with "ABC" stacking, is observed.

SAED oriented "face-on" at 0° tilt exhibits in-plane d-spacing of 6.7 Å and 5.33 Å (Figure 3 g). "Edge-on" SAED (Figure 3 j) reveals a d-spacing of 6.67 Å. Electron diffraction is consistent with WAXS and XRD of bulk powders. Indexing the powder pattern did not result in satisfactory fits for any crystal system with lower symmetry than monoclinic. Unfortunately, owing to a short life time, instability under the electron beam, and particle shape anisotropy of this phase, we have been unable to find a unique solution for the structure so far. However, a MAXS peak 26.2 Å, with harmonics at 13.1 and 6.7 Å that emerge after a period of growth, is consistent with ordered stacks of 6.7 Å thick platelets separated by interlayer water, which may account for the structural water observed in TGA and IR.

The foregoing evidence demonstrates that ABC is a highly transient precursor to a crystalline barium carbonate monohydrate that we refer to as gortatowskite. These findings show that there is a surprisingly rich chemistry hidden in plain sight in the $BaCO_3$–H_2O system. The combination of in situ techniques with high time and spatial resolution enabled deep insights into the pathway along which highly metastable precursors ABC and gortatowskite transform. Interestingly, this pathway bears strong resemblance to that observed in the calcium phosphate system,[30] inasmuch as the temporal evolution from spherical amorphous particles to ribbons, plates, and acicular spherulitic crystals is also observed to occur in the same sequence. However, in the $BaCO_3$ system these transformations occur at least three orders of magnitude faster. While the range of supersaturations over which the pathway described herein is active is still an open question, ABC and gortatowskite may frequently go undetected during the formation of barium carbonates owing to their transient existence.

References

[1] E. Nakouzi, O. Steinbock, Sci. Adv. 2016, 2, e1601144. [2] J. M. Garc&a-Ruiz, E. Melero-Garc&a, S. T. Hyde, Science 2009, DOI: https://doi.org/10.1098/rspb.2008.0192. [3] W. L. Noorduin, A. Grinthal, L. Mahadevan, J. Aizenberg, Science 2013, 340, 832. [4] C. N. Kaplan, W. L. Noorduin, L. Li, R. Sadza, L. Folkertsma, J. Aizenberg, L. Mahadevan, Science 2017, 355, 1395 – 1399. [5] J. Eiblmeier, M. Kellermeier, M. Deng, L. Kienle, J. M. Garc&aRuiz, W. Kunz, Chem. Mater. 2013, 25, 1842 – 1851. [6] J. Eiblmeier, U. Schgrmann, L. Kienle, D. Gebauer, W. Kunz, M. Kellermeier, Nanoscale 2014, 6, 14939. [7] S. E. Wolf, J. Leiterer, M. Kappl, F. Emmerling, W. Tremel, J. Am. Chem. Soc. 2008, 130, 12342 – 12347. [8] S. E. Wolf, L. Mgller, R. Barrea, C. J. Kampf, J. Leiterer, U. Panne, T. Hoffmann, F. Emmerling, W. Tremel, Nanoscale 2011, 3, 1158 – 1158. [9] S. J. Homeijer, R. A. Barrett, L. B. Gower, Cryst. Growth Des. 2010, 10, 1040 – 1052. [10] M. L. Whittaker, D. Joester, Adv. Mater. 2017, 29, 1606730 – 1606735. [11] E. Couradeau, K. Benzerara, E. Gerard, D. Moreira, S. Bernard, G. E. Brown, Jr., P. Lopez-Garcia, Science 2012, 336, 459 – 462. [12] L. Chen, Y. Shen, A. Xie, B. Huang, R. Jia, R. Guo, W. Tang, Cryst. Growth Des. 2009, 9, 743 – 754. [13] L. Addadi, S. Raz, S. Weiner, Adv. Mater. 2003, 15, 959 – 970. [14] A. V. Radha, A. Navrotsky, Cryst. Growth Des. 2015, 15, 70 – 78. [15] A. V. Matyskin, B. Ebin, M. Tyumentsev, S. Allard, G. Skarnemark, H. Rameb-ck, C. Ekberg, J. Radioanal. Nucl. Chem. 2016, 307, 1 – 7. [16] M. L. Whittaker, W. Sun, K. A. DeRocher, G. Ceder, D. Joester, Adv Funct. Mater. 2017, in press. [17] C. C. Tester, M. L. Whittaker, D. Joester, Chem. Commun. 2014, 50, 5619. [18] M. L. Whittaker, P. Dove, D. Joester, MRS Bull. 2016, 41, 388 – 392. [19] J. Bolze, B. Peng, N. Digenouts, P. Panine, T. Narayanan, M. Ballauff, Langmuir 2002, 18, 8364 – 8369. [20] G. Beaucage, J. Appl. Crystallogr. 1995, 28, 717 – 728. [21] J. Ilavsky, P. R. Jemian, J. Appl. Crystallogr. 2009, 42, 347 – 353. [22] C. M. Holl, J. R. Smyth, H. M. S. Laustsen, S. D. Jacobsen, R. T. Downs, Phys. Chem. Miner. 2000, 27, 467 – 473. [23] T. Nishino, T. Sakurai, N. Ishizawa, N. Mizutani, M. Kato, J. Solid State Chem. 1987, 69, 24 – 29. [24] R. Strobel, M. Maciejewski, S. E. Pratsinis, A. Baiker, Thermochim. Acta 2006, 445, 23 – 26. [25] V. Ischenko, J. Woltersdorf, E. Pippel, R. Kçferstein, H.-P. Abicht, Solid State Sci. 2007, 9, 303 – 309. [26] S. Ono, Phys. Chem. Miner. 2007, 34, 215 – 221. [27] N. Koga, Y. Nakagoe, H. Tanaka, Thermochim. Acta 1998, 318, 239 – 244. [28] M. M. Tlili, M. B. Amor, C. Gabrielli, S. Joiret, G. Maurin, P. Rousseau, J. Raman Spectrosc. 2002, 33, 10 – 16. [29] J. C. Meyer, A. K. Geim, M. I. Katsnelson, K. S. Novoselov, T. J. Booth, S. Roth, Nature 2007, 446, 60 – 63. [30] W. J. E. M. Habraken, J. Tao, L. J. Brylka, H. Friedrich, L. Bertinetti, A. S. Schenk, A. Verch, V. Dmitrovic, P. H. H. Bomans, P. M. Frederik, et al., Nat. Commun. 2013, 4, 1507 – 1512.